Surface Morphology and Nodule Formation Mechanism of Cellulose Acetate Membranes by Atomic Force Microscopy

Yiming Zeng, Zhigang Wang, Lijun Wan, Yanqiao Shi, Guanwen Chen, Chunli Bai

Institute of Chemistry, Chinese Academy of Sciences, Beijing 100080, People's Republic of China

Received 29 May 2002; accepted 27 June 2002
Published online 19 February 2003 in Wiley InterScience (www.interscience.wiley.com). DOI 10.1002/app.11833

ABSTRACT: By the use of atomic force microscopy (AFM), formation mechanism of nodular structure in cellulose acetate membranes was systematically investigated. Elementary factors affecting the nodule formation were delineated on the basis of both kinetic and thermodynamic considerations. It was shown that (1) the exact nature of nodular structure is thermodynamic equilibrium glassy state; nodular structure will vanish in the rubbery state; (2) the thermodynamic factor affecting nodule formation is the membrane formation temperature; with the membrane formation temperature decreasing, more chain segments are able to form nodular structures; (3) nodule formation is dependent on the segment rearrangement; variation of the solvent environment is the major kinetic factor affecting the segment rearrangement and nodule formation. © 2003 Wiley Periodicals, Inc. J Appl Polym Sci 88: 1328–1335, 2003

Key words: atomic force microscopy (AFM); membranes; surfaces

INTRODUCTION

For polymeric separation membranes, nodule formation is a commonplace occurrence. Panar et al.[1] were among the first to report on noncrystalline spheres of about 60 nm in the top layer of reverse osmosis membranes. Many other researchers also reported the presence of nodular structure in various separation membranes. Nodules were commonly believed to be paracrystalline in nature; however, they were also found in membranes made from amorphous polymers.[2,3] Wienk et al.[4] found that in PES [poly(ether sulfone)] asymmetric ultrafiltration membranes, several layers of nodule exist in the top layer, and the size of nodules is the smallest at the surface and increases deeper into the dense film. With etching the top layer of PPO [poly (2,6-dimethyl-1,4-phenylene oxide)] dense membranes by oxygen plasma, Khulbe and Matsuura[5] also discovered that the size of nodules on the top layer is smaller than the nodules in the inner layer. Nodular structures were also found in composite membranes. Cadott reported that nodules were closely packed on the surface of a fully aromatic polyamide membrane prepared by the reaction product between *m*-phenylene diamine and trimesoylchloride.[6,7]

Nodular structure plays an important role in determining the separation behavior of the membranes. Based on the sizes of nodular structures, Kesting established a structural foundation for different membrane separations: microfiltration MF, ultrafiltration UF, reverse osmosis RO, and gas seperation GS.[3] The dual distribution of pores in RO and GS membranes were also explained by the difference of density within and between nodules. Kesting suggested that nodule interiors are denser than interstitial regions; therefore, chain segment displacements within and between nodules differ, and hence constitute a bimodal pore size distribution, which may account for the dual mode sorption and permeation of gases.[3] The bimodal behavior was verified by PALS (Positron Annihilation Lifetime Spectroscopy) studies. For a wide range of glassy polymers, the presence of free volume elements in the polymeric membranes is typically bimodal.[8]

Great effort has been made to investigate the nodule formation mechanism. Several theories have been developed. (1) Some authors attributed the nodule formation to the aggregates or micelles that are initially present in the casting solution.[1] Kesting suggested that all structural elements of the membrane are built up from these aggregates.[9] However, nodules can also be obtained from moderately concentrated polymer solutions in good solvent. (2) Another theory for the generation of the nodules is that the nodules are the result of liquid–liquid demixing by nucleation and growth of a polymer-rich phase.[10] This theory does not necessarily explain nodule formation in concentrated polymer solutions. (3) A surface phenomenon

Correspondence to: C. Guanwen (gwchen@btamail.net.cn).
Contract grant sponsor: National Science Foundation of China.

TABLE I
Membrane Formation Conditions, Nodule Sizes, and Roughness Parameters

Membrane	Membrane formation temperature (°C)	Membrane formation atmosphere	*Ra* (nm)	*Rq* (nm)	*Z* (nm)	Mean size of nodules (nm)
CA-I-50	50	I	0.437	0.881	7.536	95
CA-I-34	34	I	3.332	3.970	28.940	350
CA-I-20	20	I	1.334	2.169	37.793	359
CA-I-10	10	I	8.410	10.980	72.856	550
CA-I-0	0	I	9.650	11.820	96.068	600
CA-I*-(−10)	−10	I*	6.812	8.900	88.280	570
CA-II-20	20	II	0.514	0.667	5.475	45
CA-II*-20	20	II	1.085	1.475	17.561	No

I: Acetone evaporation was completed in an atmosphere with nearly saturated acetone vapor for 72 h.
I*: Acetone evaporation was completed in an atmosphere with nearly saturated acetone vapor for 120 h.
II: Membrane formation was completed in air, and the casting ring was covered with a filter paper to keep out dust and to prevent the orange peel effect caused by rapid solvent evaporation.
CA-II*-20 membrane was obtained from CA-II-20 membrane by posttreatment. CA-II-20 membrane was first immersed in a water bath of 100°C for 30 min, and then suddenly quenched in a water bath of 20°C.

as a cause for nodule formation was also proposed, but it would not be possible to explain several layers of nodules in the dense film.[4] An interested reader is referred to refs. 4 and 11 for a detailed review of the theories proposed by previous researchers and the experiments, which are in contradiction to the theories. No experimental evidence is available to support the current theories.[11] In other words, the formation mechanism of the nodular structure has not yet been elucidated in detail.

The aim of this work is to elucidate the elementary factors affecting nodule formation. Note that nodule interiors are denser than interstitial regions;[3,14] we suggested that chain segments within the nodules are in the thermodynamic equilibrium glassy state, and the others in the nodule boundaries and interstitial regions are in the nonequilibrium glassy state. The thermodynamic driving force for the nodule formation is attributed to the decrease of configurational entropy due to solvent evaporation from the casting solution during the membrane formation process; so the basic kinetic process for the nodule formation is attributed to the segment rearrangements from the nonequilibrium glassy state to the equilibrium glassy state. AFM (atomic force microscopy) is used to comply with the main objective of observing the nodules on the top surface of the membranes. AFM is a newly developed high-resolution technique to study the surface morphology of the separation membranes.[12] It is used to obtain highly detailed topologic images with a typical resolution for membrane samples of a few nanometers, and the three dimensionality of the membrane surface can be determined directly. It provides for clearer observation of fine features like nodule boundaries and interstitial regions, which could be obscured by rough topography and could not be differentiated by scanning electron microscopy (SEM) and transmission electron microscopy (TEM). With SEM it is difficult to estimate the realistic nodule size due to the thickness of the gold-coating layer.[4] Another excellent advantage of this technique is its ability to image nonconducting materials without special sample preparation, which is essential for SEM and TEM.

EXPERIMENTAL

Membrane preparations

Cellulose acetate (53.5–55.5% acetyl content, η_0 = 0.3–0.5 Pa s) is a commercial product of Cellulose Acetate Factory, Shanghai. Cellulose acetate was dissolved in acetone at a concentration of 2.0 wt %. All casting solutions were mixed thoroughly and filtered through a 5-μm filter. Membranes were cast by pipetting 5 mL of the casting solution into a circular glass ring (7.8 cm in diameter), which was placed on a leveled glass plate. Casting conditions are comprised of the membrane formation temperature and atmosphere. They are described in detail in Table I. After the membranes were solid and relatively free of solvent, they were removed very cautiously from the glass plate by immersing the whole plate in a water bath and kept on a filter paper. The membranes were further dried for 24 h at room temperature, followed by keeping them in a vacuum desiccator for 14 days to remove last traces of the residual solvent. The thickness of CA membranes was 12 μm.

The membranes are identified in this text by a three-area code: the first area is relative to the polymer used, the second to the atmosphere (I or II), and the third is relative to the casting temperature.

AFM images

The images of the membrane surface were obtained by using TM AFM on a Nanoscope III equipped with a

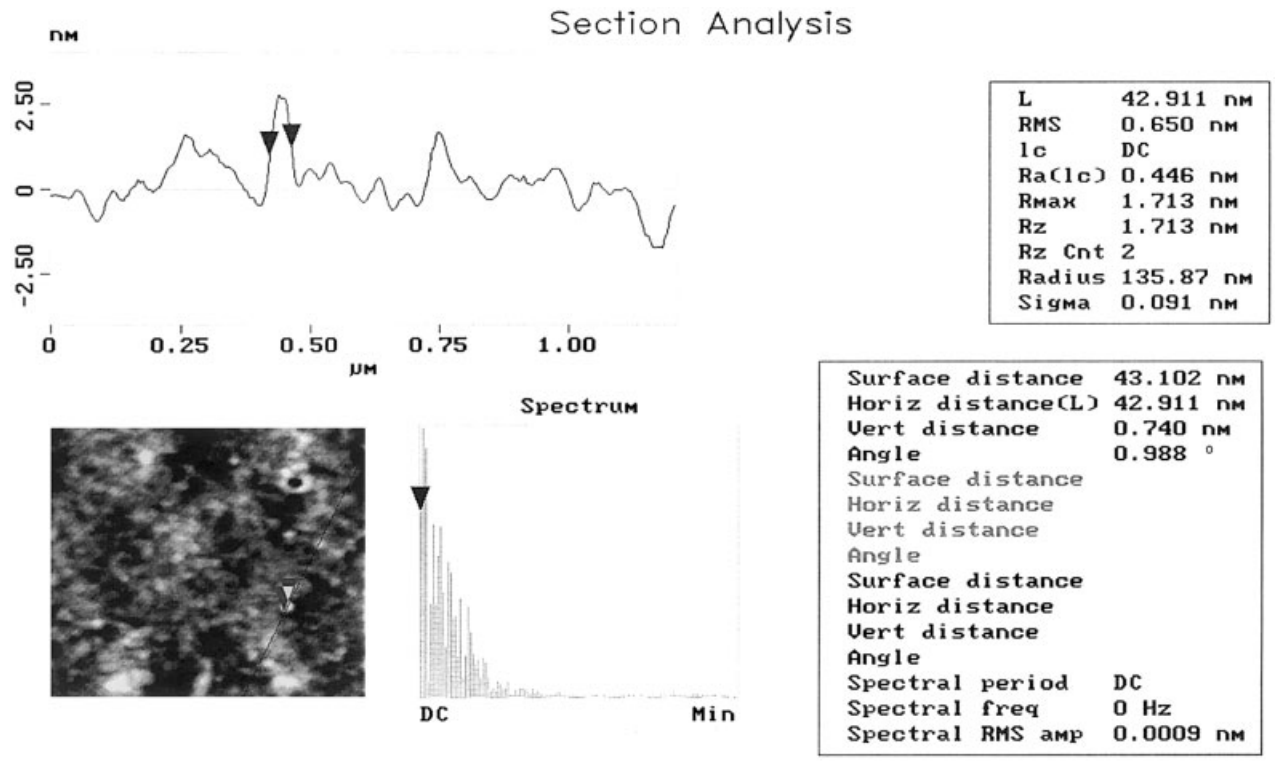

Figure 1 Section analysis of the AFM image: a vertical displacement profile of the top surface of the CA membrane.

1553D scanner from Digital Instruments, Santa Barbara, CA. The membrane surface is scanned in intermediate contact (tapping mode) with an oscillating tip. This eliminates shear forces that can damage soft samples and reduce the damage resolution. Small pieces of approximately 1-cm^2 areas were cut from each prepared membrane, glued onto freshly cleaved mica, and located on top of the scanner tube. All the TM AFM images were undertaken at 25°C.

All the surface roughness parameters are calculated from the AFM images using an AFM software program. Definitions of the roughness parameters were listed below.

1. The difference between the highest and the lowest points within the given area, z.
2. The standard deviation of the z-values within the given area (R_q). This parameter is calculated as $Rq = [\Sigma\ (Z_i - Z_{\text{avg}})2/N]^{1/2}$, where Z_i is the current z-value, Z_{avg} is the average of the Z-value within the given area, and N is the number of points within given area.
3. The mean roughness (R_a). This parameter represents the mean value of the surface relative to the center plane, the plane for which the volumes enclosed by the image above and below this plane are equal. It is calculated as

$$Ra = \frac{1}{L_x L_y}\int_0^{L_x}\int_0^{L_y} |f(x,y)| \cdot dx \cdot dy$$

where $f(x,y)$ is the surface relative to the center plane and L_x and L_y are the dimension of the surface in the x and y directions, respectively.

The roughness parameters depend on the curvature and size of the TM AFM tip as well as on the treatment of the captured surfaces data (plane fitting, flattening, filtering, etc). They should not be considered as absolute roughness values. However, in the present study, the same tip was used for all membranes, and all captured surfaces were treated in the same way.

The size of the nodules was estimated from cross-sectional profiles of the data along the reference line. An example of the measurement of the diameters of nodules is shown in Figure 1. For each pair of cursors the horizontal and vertical distances as well as the angle between the cursor are given in the right window. Because the lateral dimensions of sample structure in AFM are overestimated due to the finite dimensions of the tips, to minimize the broadening effect of AFM, we measured the diameter of nodules with full width at half-maximum height. The reported size (diameter) of the nodule is based on the average of at least 30 measurements.

RESULTS AND DISCUSSION

Characterization of the membrane surface

By comparing the AFM images, the difference of nodule size and nodule distribution on the top surface of the membranes prepared in different conditions will

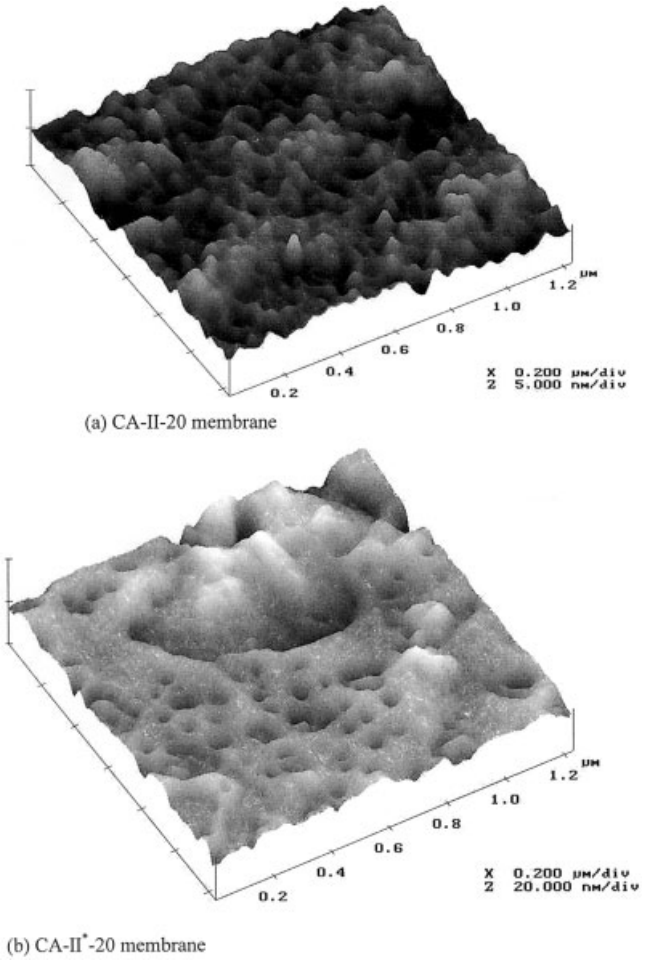

Figure 2 AFM images of the top surface of the CA membranes: (a) CA-II-20 membrane; (b) CA-II*-20 membrane.

be investigated in this section. The membrane surface morphology is always characterized by various roughness parameters, such as the mean roughness (R_a), the root-mean-square of vertical data (R_q), and the mean difference between the five highest peaks and the five lowest valleys (z). These parameters were calculated from the AFM images presented in Figures 2 and 4–9, with the use of an appropriate software program. Membrane formation conditions, average diameters of the nodules, and roughness parameters of the membranes are summarized in Table I. It is noticed that as an experimental rule, surface roughness tends to increase with increasing the nodule size.This indicates that nodule size is a factor affecting the roughness of a membrane surface.

Exact nature of the nodular structure

The AFM images of the top surface of the CA-II-20 membrane and the CA-II*-20 membrane are shown in Figure 2. There is noticeable difference between the two membranes. Figure 2(a) reveals a relatively uniform nodular structure with average diameter of approximately 45 nm. However, no nodular structure is observed on the top surface of the CA-II*-20 membrane [Fig. 2(b)]. The CA-II*-20 membrane was obtained by posttreatment of the CA-II-20 membrane. First, the CA-II-20 membrane was immersed into a water bath of 100°C for 30 min, and then suddenly quenched in a water bath of 20°C. The AFM image of the CA-II*-20 membrane should signify some characteristics of the CA-II-20 membrane at 100°C. The glass transition temperature, T_g, of CA reported in the literature is 68.6 or 80°C.[2,17] The value reported here is 94°C, determined by DSC experiment at a heating rate of 20°C · min^{-1}, taken at the midpoint of the transition heat capacity increment. The result indicates that nodular structures do not exist in the rubbery state. Note that nodule interiors are denser than nodule boundaries and interstitial regions,[3,14] and the thermodynamic state of the regions may be different. It is reasonable to infer that nodular interiors are in the thermodynamic equilibrium glassy state.

Surface roughness and nodule structure

Although nodular structure is not present on the AFM images of the top surface of the CA-II*-20 membrane, the surface roughness of the CA-II*-20 membrane is larger than that of the CA-II-20 membrane. It is reported that with increasing the nodule size the surface roughness of the membrane tends to increase.[13] Here, surface roughness is not in proportion to the nodule size. The dark depression region on the AFM image as shown in Figure 2(b) may provide a possible explanation. Both depression region and nodular structure would account for the roughness of a membrane surface. The two structures are originated from different mechanisms because the depression region is only a surface phenomenon. The depression region on the AFM image of the membrane surface was also reported in other literatures,[14,15,16] but in our review of the literature there is no reasonable explanation for its formation.

Effect of membrane formation temperature

To elucidate the elementary factors affecting nodule formation, it is a good approach to investigate its formation based on the path curve that denotes the membrane formation process in the phase diagram. Binary phase diagram of amorphous polymer–good solvent system was illustrated in Figure 3. The sol-gel transition curve and the glass transition temperature depression curve divide the phase diagram into three regions: sol, gel, and glass. Path curve OABC denotes the membrane formation process at a temperature below T_g. When solvent evaporates from the membrane formation system, configurational entropy of polymer chains will decrease and chain segments will

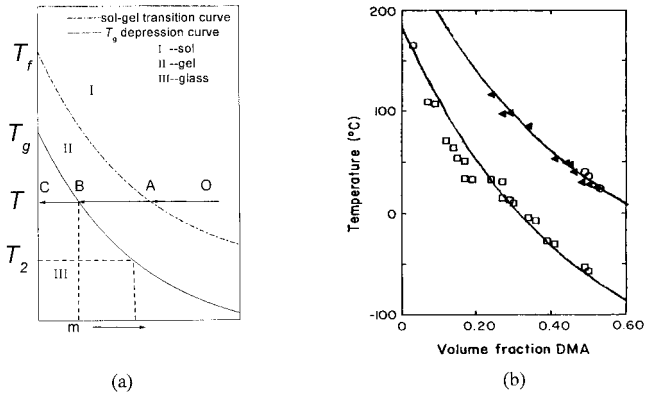

Figure 3 (a) Schematic phase diagram of the amorphous polymer–good solvent system (m: mol fraction of the solvent). (b) Experimental data of sol-gel transition and T_g depression from literature for binary PSF–DMA system.[19] The curves are simulated by equations:

$$T_g(m) = T_g \exp\{-\lambda_1 m\}$$

$$T_{gel}(m) = T_f \exp\{-\lambda_2 m\}$$

(PSF: polysulphone; DMA: *N,N*-dimethylacetamide; T_f: fusion temperature)

pack more density. The resultant membrane will attain the most stable state in thermodynamics at that temperature. According to the Gibbs-DiMarzio entropy theory,[18] the glassy state represents a situation of excess in configurational entropy, which is in a state of quasi-equilibrium; if a glass-forming liquid were cooled infinitely slow, the equilibrium glassy state would be attained at a temperature of about 50°C below T_g (T_2, second-order transition temperature), and the configurational entropy of the system equals zero. By the thermodynamic prediction, with decreasing the membrane formation temperature excess configulational entropy of the resultant membrane decreases until at T_2 equals zero. That means more and more chain segments will transfer to form nodular structure with the membrane formation temperature decreasing until at T_2.

Table I shows that nodule size tends to increase when membrane formation temperature decreases from 50 to 10°C. Below 10°C, the average diameters of the nodules on the top surface of the membranes are similar. AFM images further reveal the difference of interstitial regions on the top surface of each membrane (Figs. 4–7). The bright objects are isolated from each other on the AFM image of CA-I-50 membrane (Fig. 4). One can clearly identify the nodule boundaries and interstitial regions. Interstitial regions are larger than the sum area of nodular structures. Isolated nodular structures are also present on the AFM images of the CA-I-34 membrane and the CA-I-20 membrane. Compared with the CA-I-50 and CA-I-20 membranes, the surface roughness of the CA-I-34

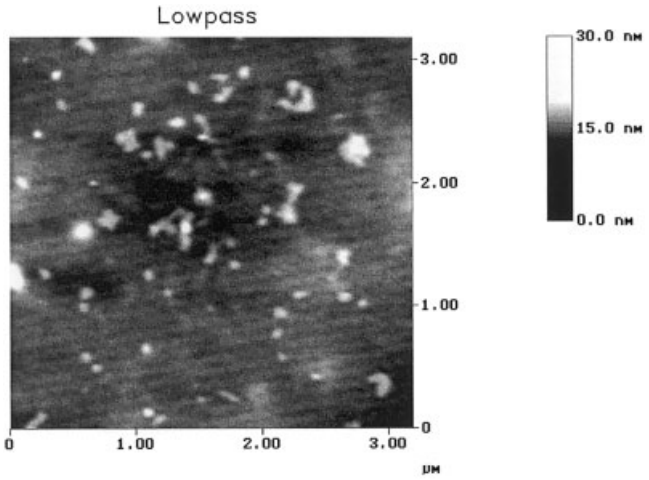

CA-I-50 membrane

Figure 4 AFM image of the top surface of the CA-I-50 membrane.

membrane is larger. With the same reason discussed above, the dark depression regions on the AFM image as shown in Figure 5 may be a possible reason. Due to the existence of the dark depression regions, the distribution of nodular structures is obscure. On the AFM image of the CA-I-20 membrane, few dark depression regions are present on the membrane surface. The isolated nodules, distinct boundaries, and interstitial regions can be clearly identified. On the AFM image of the CA-I-10 membrane (Fig. 6), nodular structures are packed closely on the membrane surface, and no interstitial region is observed. Few dark depression re-

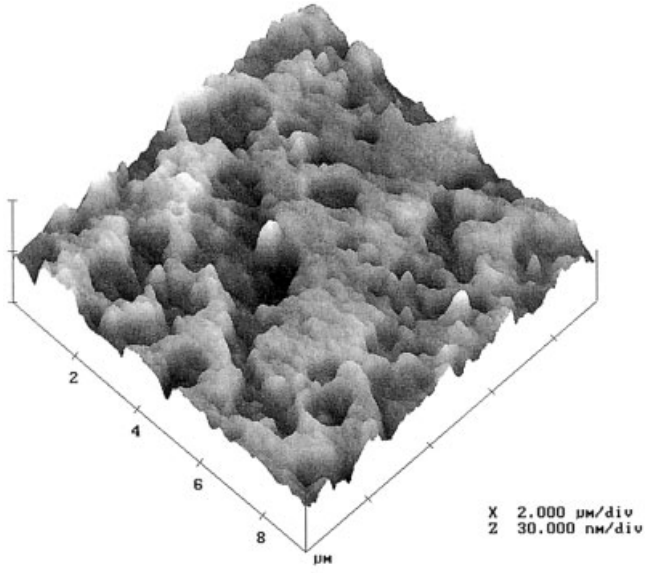

CA-I-34 membrane

Figure 5 AFM image of the top surface of the CA-I-34 membrane.

gions are present on the top surface of the CA-I-50, CA-I-20, and CA-I-10 membranes, and the effect of membrane formation temperature on nodule size and nodule distribution can be illustrated by comparison of the AFM images of the three membranes. It is obvious that with the decrease of membrane formation temperature, interstitial regions tend to decrease, until at 10°C no interstitial region is observed on the membrane surface.

Membrane formation of these membranes was completely in an atmosphere with nearly saturated acetone vapor; the difference of the membrane surface, such as nodule size and nodule distribution, could be attributed to the membrane formation temperature. By the thermodynamic analysis presented above, the results can be explained by the dependence of the excess configurational entropy of resultant membrane on the membrane formation temperature. Configurational entropy of resultant membrane is only a function of temperature. It decreases with decreasing temperature, until at T_2 equals zero. By theoretical prediction, nodule interiors are in an equilibrium glassy state, while nodule boundaries and interstitial regions are in a nonequilibrium glassy state. The presence of interstitial regions on the top surface of the resultant membranes could be explained by the entropy theory that beyond T_2 a part of chain segments exist as a nonequilibrium glassy state. With temperature decreases, more chain segments will transfer to form the equilibrium glassy state, so the average diameter of nodules increases while the area of interstitial regions decreases.

The AFM images of the top surface of the CA-I-10, CA-I-0, CA-I*-(-10) membranes have a common characteristic; nodular structures are closely packed on each membrane surface, and no interstitial region is observed on the AFM images. The result is consistent with the theoretical prediction that below T_2 no interstitial region is present on the membrane surface. Average diameters of nodules on the AFM images of the three membranes are similar (Table I). This indicates that nodule aggregation was not complete. Nodule formation is a kinetic process; it is dependent on segment rearrangements. Solvent environment has a great effect on the segment adjustments. A possible explanation for the incomplete aggregation is that when adjacent nodules contact with each other, the remaining solvent is too finite to provide a solvent environment for segment rearrangement. The aggregation process is too slow to be observed during the experimental time. On the AFM images (Figs. 7, 8, and 9), one can identify some adjacent nodules that partly overlap each other, and nodule boundaries are obscure due to the incomplete aggregation.

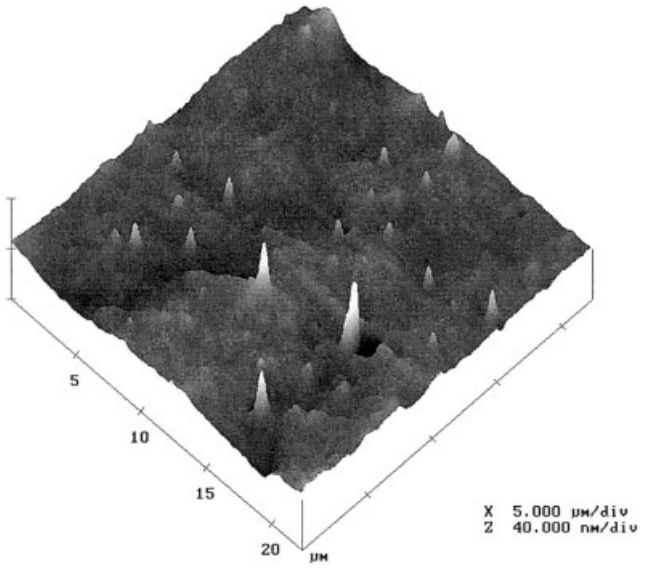

Figure 6 AFM image of the top surface of the CA-I-20 membrane.

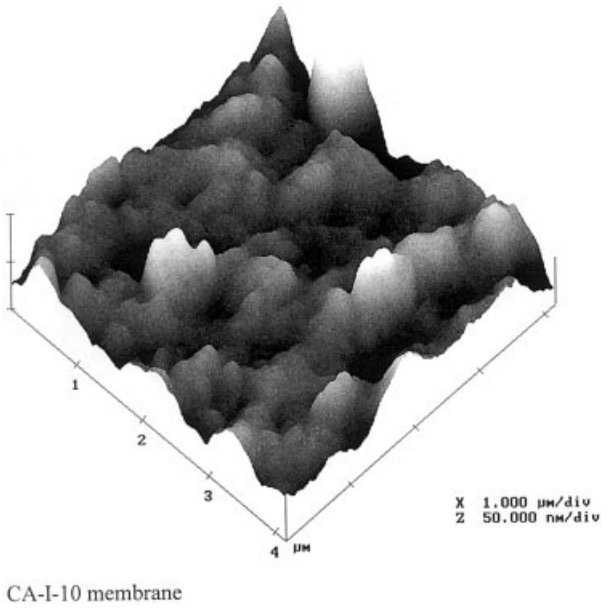

Figure 7 AFM image of the top surface of the CA-I-10 membrane.

Aggregation mechanism

With the nodular structure as the thermodynamic equilibrium glassy state, its formation is a kinetic process. A general scheme will be postulated here. First, due to solvent evaporation, configurational entropy of the polymer chains will decrease during the membrane formation process; chain segments will rearrange their configurations from the nonequilibrium state to a more equilibrium state; to minimize the interfacial area of the system, chain segments in the equilibrium state will further aggregate to form minimum nodules; and then the minimum nodules will

aggregate to form larger nodular structures by rearrangement of chain segments at nodule boundaries and interstitial regions to minimize the interfacial area of the nodular structure. Two factors account for the thermodynamic driving force of the kinetic process: the decrease of configurational entropy, and the minimization of interfacial energy. As long as chain segments are able to adjust their configurations, the process will happen. Segment rearrangement is greatly affected by the solvent environment. For the membrane formation in the lab or in industry, solvent diffusion may be very complex, and the aggregation process will stop at different stages due to loss of solvent environment or in-diffusion of nonsolvent. To predict nodule formation exactly, both out-diffusion of solvent and in-diffusion of nonsolvent should be considered carefully.

The effect of solvent evaporation on nodule formation is illustrated by comparing the AFM images of the CA-I-20 and CA-II-20 membranes. The nodules on the top surface of the CA-II-20 membrane (45 nm) are smaller than the nodules on the top surface of the CA-I-20 membrane (559 nm) (Table I). Membrane formation atmosphere of the two membranes are different: CA-I-20 membranes in a nearly saturated acetone vapor, and CA-II-20 membrane in air. Solvent evaporation rate in the forming process of the CA-II-20 membrane is faster than that of the CA-I-20 membrane. As soon as the membrane formation system loss the solvent environment, chain segments will loss mobility and cannot further adjust their configurations. For the loss of solvent environment is too fast during the formation process of the CA-II-20 membrane, and nodule aggregation will stop at an intermediate stage. But for the formation process of the CA-I-20 membrane, out-diffusion of solvent is enough slow due to the presence of the solvent atmosphere nodular structures that can aggregate to form larger structures. The result verifies that the variation of solvent environment is an elementary factor affecting the kinetic process of nodule formation.

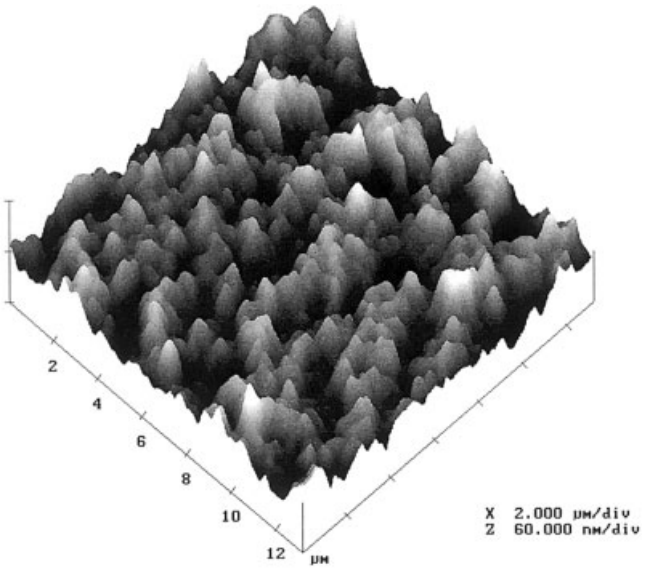

CA-I-0 membrane

Figure 8 AFM image of the top surface of the CA-I-0 membrane.

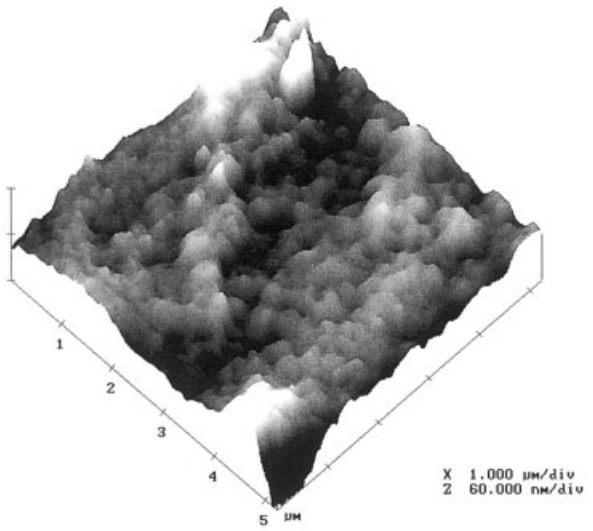

CA-I*-(-10) membrane

Figure 9 AFM image of the top surface of the CA-I*-(-10) membrane.

Besides the aggregation mechanism, liquid–liquid demixing by nucleation and growth of a polymer-rich phase was also postulated as a reason for the nodule formation. It has been pointed out that the theory fails to explain some experiments.[11] Here we add that the nucleation-growth mechanism is not suitable to explain the surface morphology of the membranes presented here. The surface morphology where large nodules are agglomerates of smaller nodules is clearly identified on the AFM image of CA-I-50 membrane (Fig. 4). It is especially clearly seen that some large bright objects consist of several smaller bright objects. This kind of surface morphology is caused by incompleteness of nodule aggregation. Similar surface morphology was also reported in the literature.[5] By the nucleation-growth mechanism, as soon as the grow fronts of the neighbor nuclei collide with each other, the growth process will stop due to the loss of thermodynamic driving force. The surface morphology presented here cannot occur.

CONCLUSIONS

Based on Kesting's suggestion that nodule interiors are denser than interstitial regions and chain segment displacements within and between nodules differ,[3] in

this article we tried to establish a thermodynamic foundation for this structure characteristics to explain the nodule formation. It was illuminated that (1) the exact nature of the nodular structure is the thermodynamic equilibrium glassy state; the nodular structure will disappear in the rubbery state; (2) the thermodynamic factor affecting the nodule formation is the membrane formation temperature; with a decrease of the membrane formation temperature, more chain segments are able to form nodular structures; (3) segment rearrangement is a basic kinetic process for the nodule formation; solvent environment is a major factor affecting the segment rearrangement; for the formation of dense membranes, with the increase of evaporation rate, the diameter of the nodules tend to decrease.

References

1. Panar, M.; Hoehn, H. H.; Hebert, R. R. Macromolecules 1973, 6, 777.
2. Kesting, R. E. Synthetic Polymeric Membranes: A Structural Perspective; Wiley-Interscience: New York, 1985, 2nd ed.
3. Kesting, R. E. J Appl Polym Sci. 1990, 41, 2739.
4. Wienk, I. M.; van den Boomgaard, Th.; Smolders, C. A. J Appl Polym Sci 1994, 53,1011.
5. Khulbe, K. C.; Matsuura, T. J Membr Sci 2000, 171, 273.
6. Cadott, J. U.S. Pat. 4277344 (1981).
7. Cadott, J. ACS Symp Ser 1985, 269, 273.
8. Shantarovich, V. P.; Kevdina, I. B.; Yampolskii, Yu. P.; Alentiev, A. Yu Macromolecules 2000, 33, 7453.
9. Kesting, R. E. ACS Symp Ser 1985, 269, 131.
10. Kamide, K.; Iijima, H.; Matsuda, S. Polym J 1993, 25, 1113.
11. van de Witte, P.; Dijkstra, P. J.; Van den Berg, J. W. A.; Feijen, J. J Membr Sci 1996, 117, 1.
12. Khulbe, K. C.; Matsuura, T. Polymer 2000, 41,1917.
13. Khulbe, K. C.; Matsuura, T.; Noh, S. H. J Membr Sci 1998, 145, 243.
14. Khulbe, K. C.; Kruczek, B.; Chowdhury, G.; Gagne, S.; Matsuura, T. J Appl Polym Sci 1996, 59, 1151.
15. Stamatialis, D. F.; Dias, C. R.; de Pinho, M. N. J Membr Sci 1999, 160, 235.
16. Lehmani, A.; Durand-Vidal, S.; Turq, P. J Appl Polym Sci 1998, 68, 503.
17. Mulder, M. Basic Principles of Membrane Technology; Kluwer Academic Publishers: The Netherlands, 1996.
18. Gibbs, J. H.; DiMarzio, E. A. J Chem Phys 1958, 28, 373.
19. Gaides, G. E.; McHugh, A. J. Polymer 1989, 30, 2118.